AGU PUBLICATIONS

Paleoceanography

RESEARCH ARTICLE
10.1002/2014PA002677

Key Point:
- Southern Westerly Winds, Brazil-Malvinas Confluence, Holocene

Correspondence to:
I. Voigt,
ivoigt@marum.de

Citation:
Voigt, I., C. M. Chiessi, M. Prange, S. Mulitza, J. Groeneveld, V. Varma, and R. Henrich (2015), Holocene shifts of the southern westerlies across the South Atlantic, *Paleoceanography*, *30*, doi:10.1002/2014PA002677.

Received 30 MAY 2014
Accepted 12 JAN 2015
Accepted article online 15 JAN 2015

Holocene shifts of the southern westerlies across the South Atlantic

Ines Voigt[1], Cristiano M. Chiessi[2], Matthias Prange[1], Stefan Mulitza[1], Jeroen Groeneveld[1], Vidya Varma[3], and Ruediger Henrich[1]

[1]MARUM–Center for Marine Environmental Sciences and Faculty of Geosciences, University of Bremen, Bremen, Germany, [2]School of Arts, Sciences and Humanities, University of São Paulo, São Paulo, Brazil, [3]Department of Meteorology, Stockholm University, Stockholm, Sweden

Abstract The southern westerly winds (SWW) exert a crucial influence over the world ocean and climate. Nevertheless, a comprehensive understanding of the Holocene temporal and spatial evolution of the SWW remains a significant challenge due to the sparsity of high-resolution marine archives and appropriate SWW proxies. Here we present a north-south transect of high-resolution planktonic foraminiferal oxygen isotope records from the western South Atlantic. Our proxy records reveal Holocene migrations of the Brazil-Malvinas Confluence (BMC), a highly sensitive feature for changes in the position and strength of the northern portion of the SWW. Through the tight coupling of the BMC position to the large-scale wind field, the records allow a quantitative reconstruction of Holocene latitudinal displacements of the SWW across the South Atlantic. Our data reveal a gradual poleward movement of the SWW by about 1–1.5° from the early to the mid-Holocene. Afterward, variability in the SWW is dominated by millennial scale displacements on the order of 1° in latitude with no recognizable longer-term trend. These findings are confronted with results from a state-of-the-art transient Holocene climate simulation using a comprehensive coupled atmosphere-ocean general circulation model. Proxy-inferred and modeled SWW shifts compare qualitatively, but the model underestimates both orbitally forced multimillennial and internal millennial SWW variability by almost an order of magnitude. The underestimated natural variability implies a substantial uncertainty in model projections of future SWW shifts.

1. Introduction

The southern westerly winds (SWW) and their associated storm tracks dominate the midlatitude dynamics of the Southern Hemisphere atmosphere and influence the extratropical large-scale temperature and precipitation patterns [*Thompson and Solomon*, 2002; *Garreaud*, 2007]. Changes in the strength and/or the position of the SWW may affect the ocean circulation through the impact on the Antarctic Circumpolar Current and the wind-driven upwelling of deep water in the Southern Ocean [*Toggweiler and Samuels*, 1995; *Sijp and England*, 2008]. So far, there is surprisingly little systematic knowledge about orbital to millennial scale changes of the SWW during the Holocene (11.5 ka B.P. to the present). Available reconstructions of the paleo-SWW which are primarily based on precipitation/moisture proxies and their correlation to wind changes reach contradicting conclusions with respect to the strength and/or position of the SWW over the Holocene [*Fletcher and Moreno*, 2012; *Kilian and Lamy*, 2012]. For the mid-Holocene, for instance, some studies indicate a northward displacement and/or increased intensity of westerly flow (relative to the early Holocene) [e.g., *Shulmeister*, 1999; *Jenny et al.*, 2003; *Moreno*, 2004; *Shulmeister et al.*, 2004; *Moreno et al.*, 2010]; whereas, others show a southward displacement and/or weaker intensity of westerly flow [e.g., *Nicholson and Flohn*, 1980; *Moros et al.*, 2009]. These inconsistencies have been, at least partly, attributed to unclear relations between paleoprecipitation and the mean westerly winds, restricted proxy understanding, and/or unavailable proxy calibration [*Kilian and Lamy*, 2012; *Kohfeld et al.*, 2013; *Sime et al.*, 2013]. Hence, this issue is still a matter of discussion, and consensus remains elusive. Therefore, new approaches are required to address paleo-SWW variability throughout the Holocene.

Despite its importance, relatively few studies directly address Holocene changes of westerly winds in the Atlantic sector. For this purpose, we focus on the Brazil-Malvinas Confluence (BMC), a prominent feature of the upper level circulation in the western South Atlantic which responds sensitively to changes in the position of the SWW [*Peterson and Stramma*, 1991; *Matano et al.*, 1993; *Sijp and England*, 2008; *Lumpkin and*

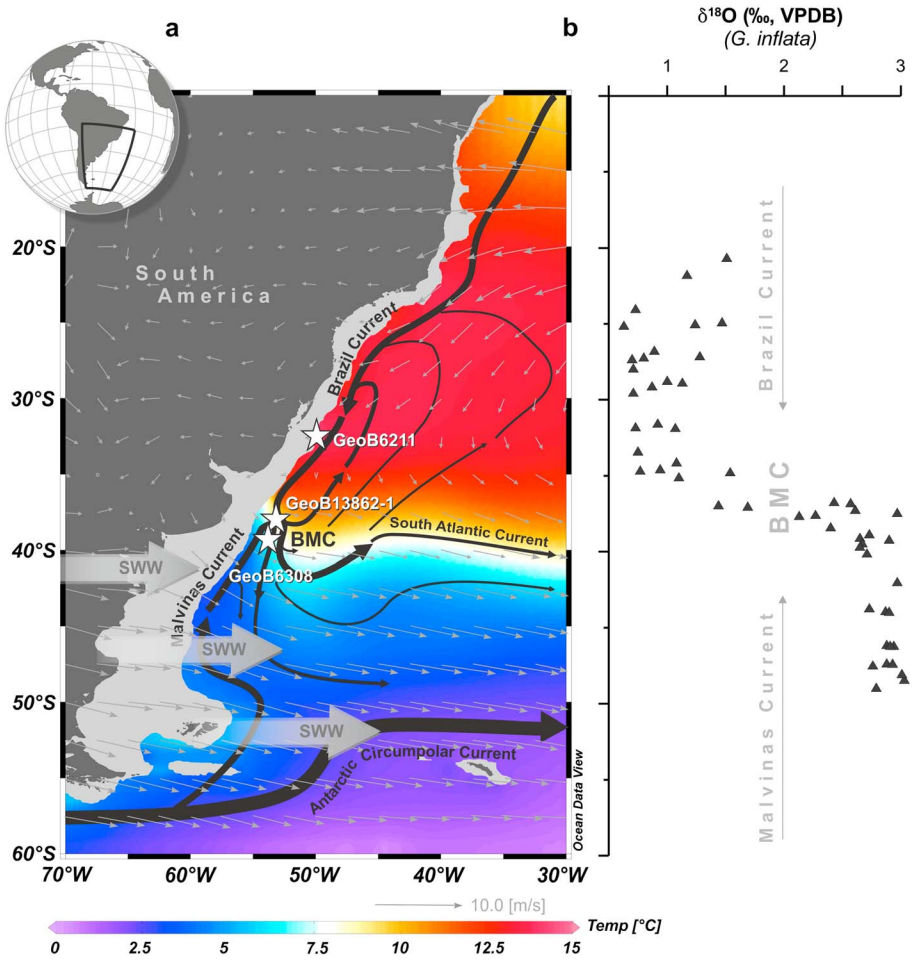

Figure 1. Modern annual mean temperature and surface winds in the western South Atlantic. (a) The color chart represents annual mean temperature (°C) at 350 m water depth (WOA09), within the apparent calcification depth of planktonic foraminifera *Globorotalia inflata* in the South Atlantic [*Groeneveld and Chiessi*, 2011]. The black arrows indicate upper level ocean circulation [*Peterson and Stramma*, 1991]. The thin gray arrows indicate the annual mean zonal wind based on NCEP/NCAR reanalysis data [*Kalnay et al.*, 1996]. The thick gray arrows depict the position of the southern westerly winds (SWW). The white stars show the position of the investigated sediment cores. Site GeoB13862-1 is ideally situated to monitor past changes in upper level circulation because it is located approximately beneath the modern mean position of the Brazil-Malvinas Confluence (BMC) that separates colder subpolar waters to the south from warmer subtropical waters to the north. (b) Signature of the BMC in the oxygen isotopic composition ($\delta^{18}O$) of *G. inflata* from surface sediments [*Chiessi et al.*, 2007].

Garzoli, 2011] (Figure 1). We investigated a north-south transect of three marine sediment cores from the midlatitudes of the western South Atlantic (Figure 1 and Table 1) covering the modern extent of the BMC. This enabled us to reconstruct the meridional variability of the BMC in response to latitudinal changes in the position of the SWW throughout the Holocene.

2. Modern Setting

2.1. The Brazil-Malvinas Confluence

The BMC is characterized by the encounter of the southward flowing Brazil Current (BC) and the northward flowing Malvinas (Falkland) Current (MC) [*Peterson and Stramma*, 1991] (Figure 1). This encounter takes place at approximately 38°S, generating one of the most energetic regions of the world ocean. The subantarctic waters of the MC and the subtropical waters of the BC collide in the upper 800 m of the water column, which make the BMC a major ventilation area for much of the South Atlantic thermocline [*Gordon*, 1981]. The

Table 1. Location of Sediment Cores

Core ID	Latitude	Longitude	Water Depth (m)
GeoB6211	32.5052°S	50.2427°W	657
GeoB13862-1	38.0185°S	53.7450°W	3588
GeoB6308	39.3017°S	53.9650°W	3620

combined flow of the two currents causes a strong thermohaline frontal zone characterized by sharp temperature and salinity gradients. A marked seasonal variability in the location of the BMC of up to 900 km along the continental shelf break has been described from satellite [*Olson et al.*, 1988; *Goni and Wainer*, 2001; *Saraceno et al.*, 2004] and (sub) surface observations [*Garzoli and Bianchi*, 1987; *Olson et al.*, 1988; *Garzoli and Garraffo*, 1989]. Numerical studies indicate that the seasonality of the position of the BMC is governed by seasonal north-south displacements of the South Atlantic wind stress pattern [*Matano et al.*, 1993]. Accordingly, during austral summer, the BMC reaches its southernmost position, while during austral winter, it reaches its northernmost position (Figure 2). In addition to the seasonal variability, strong interannual variability forced by anomalous wind patterns south of the confluence has also been described [*Garzoli and Giulivi*, 1994]. A recent (1992–2007) southward shift of -0.6 to $-0.9°$ decade^{-1} in the BMC latitude is suggested as a direct response to a southward shift in the maximum of the wind stress curl across the South Atlantic basin associated with a weakening of the northern portion of the SWW [*Lumpkin and Garzoli*, 2011].

Lumpkin and Garzoli [2011] show that seasonal to decadal variability in the latitude of the confluence is governed by large-scale atmospheric dynamics, more precisely by the latitude of the maximum wind stress curl across the South Atlantic basin which is linked to the northern portion of the SWW. Due to the close relationship between the South Atlantic wind field and the position of the BMC, it has been suggested that the latitude of the maximum wind stress curl can serve as a proxy for the latitude of the BMC at longer time scales [*Oke and England*, 2004; *Sijp and England*, 2008; *Lumpkin and Garzoli*, 2011]. The tight coupling between the BMC and the regional South Atlantic wind field in combination with the steep meridional thermohaline gradient assigns the confluence a great potential for reconstructing past variations of the SWW.

2.2. Planktonic Foraminifera δ^{18}O as a Proxy for the Position of the Brazil-Malvinas Confluence

We used the stable oxygen isotopic composition (δ^{18}O) of the deep-dwelling planktonic foraminifera *Globorotalia inflata* as a proxy for the position of the BMC [*Chiessi et al.*, 2007] (Figure 1). This species commonly occurs in high amounts from subtropical to subpolar conditions with an apparent calcification depth of 350–400 m in the South Atlantic [*Groeneveld and Chiessi*, 2011] and is therefore relatively less sensitive to seasonal and other short-term variations of the BMC than surface-dwelling species of foraminifera

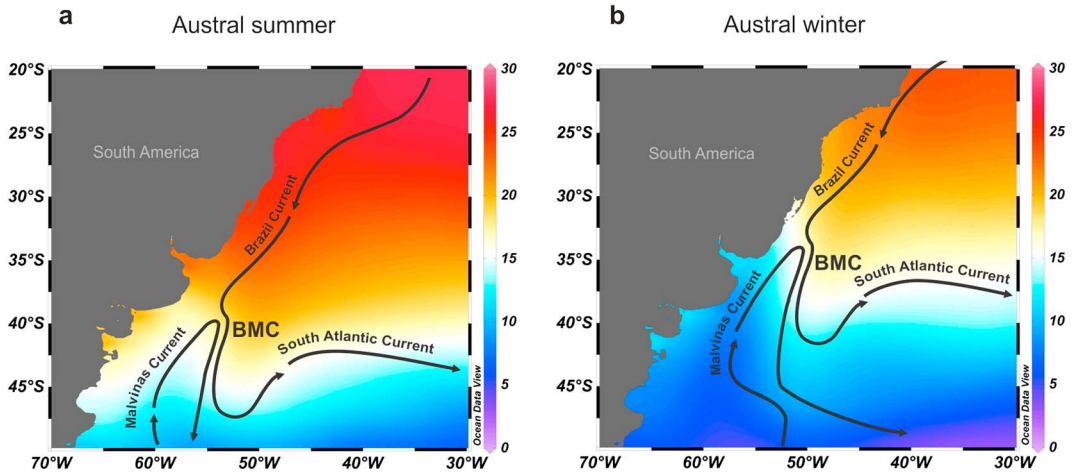

Figure 2. Seasonal mean sea surface temperature (°C) in the western South Atlantic with emphasis to the Brazil-Malvinas Confluence (BMC), (WOA09). (a) Southward shifted BMC during austral summer (January–March). (b) Northward shifted BMC during austral winter (July–September). The black arrows indicate the upper level ocean circulation [*Peterson and Stramma*, 1991]. The figures were made using Ocean Data View (http://odv.awi.de).

[*Chiessi et al.*, 2007]. Figure 1 shows the oxygen isotopic composition of *G. inflata* from modern surface samples of the western South Atlantic encompassing the BMC [*Chiessi et al.*, 2007]. The $\delta^{18}O$ of *G. inflata* depicts a sharp gradient of 2‰ at the confluence with remarkably stable values north and south of the BMC. *Chiessi et al.* [2007] suggested therefore the oxygen isotopic composition of *G. inflata* as the most reliable indicator for the present position of the BMC, which can be used to derive past migrations of the front. Further, quantitative estimates of the deviation from the BMC's modern position (in degrees of latitude) can be obtained by using the modern $\delta^{18}O$ gradient across the BMC [*Chiessi et al.*, 2007] and the ice volume corrected $\delta^{18}O$ ($\delta^{18}O_{ivc}$) record of GeoB13862-1 (as this site is located approximately beneath the modern mean position of the BMC; Figure 1) (see Materials and Methods).

It is worthy of note, though, that an oceanic area like the BMC is highly dynamic [*Peterson and Stramma*, 1991]. This potentially results in $\delta^{18}O$ of *G. inflata* that are much more variable than in stable open ocean areas [e.g., *Groeneveld and Chiessi*, 2011]. The large variability under the BMC can be assessed by calculating the standard deviation of *G. inflata* $\delta^{18}O$ from bins of five adjacent core tops of the data set published in *Chiessi et al.* [2007]. The average standard deviation for bins originating from the BMC is 0.47‰, while bins to the north and to the south of the BMC result in significantly smaller values (0.23 and 0.10‰, respectively). Accordingly, the gradient we used to reconstruct variations in the past position of the BMC denotes an idealized case. Nevertheless, we are confident that the reconstructed long-term variations of the BMC shown here are representative, since the amplitude of the downcore changes (up to 2‰) are larger than the core top variability under the influence of the BMC (0.47‰).

3. Materials and Methods

We investigated a north-south transect of three marine sediment cores (GeoB6211, GeoB13862-1, and GeoB6308) from the midlatitudes of the western South Atlantic (Figure 1 and Table 1) covering the modern extent of the BMC. The cores were collected during the following research cruises of the German research vessel *Meteor*: *M*46/2 [*Schulz et al.*, 2001], *M*46/3 [*Bleil et al.*, 2001], and *M*78/3 [*Krastel and Wefer*, 2012] (Table 1).

3.1. Age Model

All three sediment cores investigated in this study have age models based on ^{14}C accelerator mass spectrometry (AMS) analyses obtained on planktonic foraminifera (Table 2). Composite record GeoB6211 was produced merging the gravity core GeoB6211-2 and the companion multicore GeoB6211-1 [*Schulz et al.*, 2001]. Parts of the ^{14}C ages to produce the age model of GeoB6211 as shown here were originally published in *Chiessi et al.* [2008], a second part in *Razik et al.* [2013], and a third part in *Chiessi et al.* [2013]. The age model for GeoB13862-1 [*Krastel and Wefer*, 2012] was already published by *Voigt et al.* [2013]. Composite record GeoB6308 was produced merging the gravity core GeoB6308-3 and the companion multicore GeoB6308-1 [*Bleil et al.*, 2001]. The age model for GeoB6308 is based on previously published (GeoB6308-3) [*Lantzsch et al.*, 2014] and new (GeoB6308-1) ^{14}C AMS analyses performed on monospecific samples of the planktonic foraminifer *G. inflata* (Table 2). To produce the composite records, we synchronized each gravity core with its respective multicore based on the ^{14}C AMS results.

Calibration of the conventional radiocarbon ages was performed with CALIB 6.0 by applying the Marine09 calibration curve [*Reimer et al.*, 2009] and no ΔR. Age models were obtained by linear interpolation of calibrated ages. Modeled reservoir ages (http://www.reservoirage.uni-bremen.de) [*Franke et al.*, 2008] suggest that reservoir age may vary by ±100–200 years across the frontal zone, which might cause stratigraphic uncertainties while comparing our three records. The fact that our northern core (i.e., GeoB6211) was dated with shallow-dwelling foraminifera (i.e., *Globigerinoides ruber*/*Globigerinoides sacculifer*), while our two southern cores (i.e., GeoB13862-1 and GeoB6308) were dated with deep-dwelling foraminifera (i.e., *G. inflata*) might cause some additional stratigraphic uncertainties because of a local offset of ±100–150 years between the surface/mixed layer and 350–400 m water depth (i.e., the apparent calcification depth of *G. inflata* in the South Atlantic [*Groeneveld and Chiessi*, 2011]). Altogether, stratigraphic uncertainties could potentially have some effect over intercore comparisons based on centennial scale variations. For longer time scales, in particular for the long-term orbital trends described here, potential changes in the reservoir ages across the BMC or at different water depths in the upper water column seem to be negligible.

Table 2. Accelerator Mass Spectrometry (AMS) Radiocarbon Dates and Calibrated Ages Used in the Age-Depth Models of Sediment Cores GeoB6211, GeoB13862-1, and GeoB6308

Sample Code	Core Depth (cm)			Species	Radiocarbon Age ± 1σ Error (B.P.)	2σ Calibrated Age Range (cal B.P.)	Calibrated Age, Interpolated From 2σ Range (ka B.P.)
	Composite Core	Multicore	Gravity Core				
				Core GeoB6211			
Poz43428[a]	2	2	-	*G. ruber/G. sacculifer*	modern	modern	modern
Poz43429[a]	16	16	-	*G. ruber*	585 ± 25	137–284	0.21
Poz43431[a]	31	31	-	*G. ruber*	1,075 ± 30	558–690	0.62
Poz43432[a]	45	45	-	*G. ruber*	1,575 ± 30	1,049–1,227	1.14
KIA30528[a]	47	-	18	*G. ruber/G. sacculifer*	1,685 ± 30	1,169–1,299	1.23
KIA35166[a]	64	-	35	*G. ruber/G. sacculifer*	3,170 ± 40	2,839–3,105	2.97
KIA35165[a]	84	-	55	*G. ruber/G. sacculifer*	4,625 ± 45	4,763–4,973	4.87
KIA30527[a]	102	-	73	*G. ruber*	7,145 ± 55	7,506–7,730	7.62
NOSAMS75186[a]	115	-	86	*G. ruber/G. sacculifer*	9,370 ± 40	10,136–10,324	10.25
KIA35163[a]	124	-	95	*G. ruber/G. sacculifer*	9,920 ± 70	10,630–11,097	10.85
-	127	-	98	-	-	-	10.83[e]
KIA35162[a]	130	-	101	*G. ruber/G. sacculife4*	9,810 ± 110	10,493–11,084	10.80
KIA30526[a]	152	-	123	*G. ruber/G. sacculifer*	12,600 ± 70	13,812–14,254	14.05
				Core GeoB13862-1			
Poz-38071[b]	-	-	143	*G. inflata*	1,790 ± 140	1,050–1,668	1.36
Poz-42354[b]	-	-	258	*G. inflata*	4,000 ± 50	3,852–4,152	4.00
Poz-38072[b]	-	-	393	*G. inflata*	5,380 ± 60	5,612–5,886	5.75
Poz-42355[b]	-	-	490	*G. inflata*	5,840 ± 80	6,057–6,434	6.25
Poz-42356[b]	-	-	556	*G. inflata*	6,140 ± 50	6,440–6,700	6.57
Poz-38074[b]	-	-	669	*G. inflata*	8,530 ± 70	8,994–9,363	9.18
Poz-38075[b]	-	-	793	*G. inflata*	9,740 ± 70	10,460–10,827	10.64
				Core GeoB6308			
Poz-42364[c]	2	2	-	*G. inflata*	750 ± 70	270–499	0.38
Poz-42363[c]	11	11	-	*G. inflata*	1,310 ± 30	769–924	0.85
Poz-43433[d]	13	-	4	*G. inflata*	1,500 ± 30	958–1,142	1.05
Poz-43435[d]	25	-	16	*G. inflata*	2,770 ± 30	2,358–2,618	2.49
Poz-43436[d]	37	-	28	*G. inflata*	3,645 ± 30	3,445–3,637	3.54
Poz-43437[d]	495	-	405	*G. inflata*	4,490 ± 35	4,564–4,803	4.68
Poz-43438[d]	61	-	52	*G. inflata*	5,240 ± 25	5,552–5,672	5.61
Poz-43439[d]	73	-	64	*G. inflata*	6,290 ± 40	6,642–6,861	6.75
Poz-43440[d]	85	-	76	*G. inflata*	7,310 ± 40	7,667–7873	7.77
Poz-43441[d]	97	-	88	*G. inflata*	8,970 ± 40	9,518–9776	9.65
Poz-43442[d]	109	-	100	*G. inflata*	9,930 ± 50	10,676–11,087	10.9
Poz-43443[d]	116	-	107	*G. inflata*	10,130 ± 50	11,050–11,227	11.15

[a] *Chiessi et al.* [2008], *Razik et al.* [2013], and *Chiessi et al.* [2013].
[b] *Voigt et al.* [2013].
[c] ^{14}C ages being first published in this study.
[d] *Lantzsch et al.* [2014].
[e] Interpolated value between the ^{14}C ages at 95 and 101 cm depth.

3.2. Stable Oxygen Isotope Analyses

For each sample, approximately 10 specimens of *G. inflata* were selected. Evidences for changes in shell chemistry of *G. inflata* by addition of secondary calcite during the final phase of their ontogenetic cycle highlight the importance of a careful selection of individual *G. inflata* specimens when producing downcore geochemical records [*Lončarić et al.*, 2006; *Groeneveld and Chiessi*, 2011]. To reduce the potential bias caused by different size fractions and states of encrustation [*Groeneveld and Chiessi*, 2011], we selected only nonencrusted specimens of *G. inflata* in the size range between 315 and 400 μm with three chambers in the final whorl.

Stable oxygen isotopes were analyzed on a Finnigan MAT 251 mass spectrometer coupled to an automated carbonate preparation device at the Department of Geosciences, University of Bremen. The isotopic composition of the carbonate sample was measured on the CO_2 gas produced by the reaction of foraminiferal carbonate with phosphoric acid at a constant temperature of 75°C. For all stable oxygen isotope measurements, a working standard (Burgbrohl CO_2 gas) was used, which was calibrated against Vienna Pee Dee Belemnite (VPDB) by using

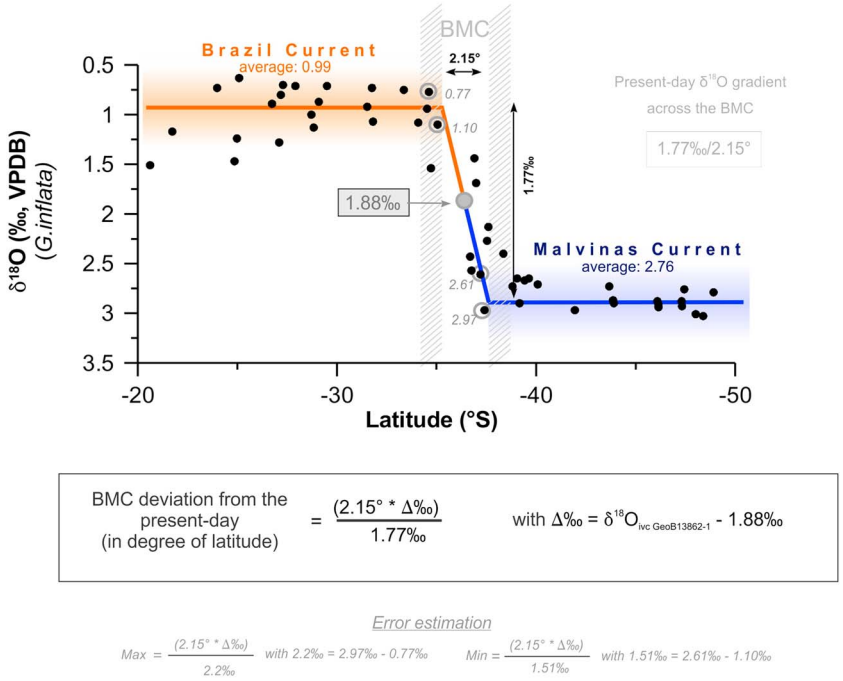

Figure 3. The $\delta^{18}O$ of *Globorotalia inflata* from a latitudinal transect of 56 surface sediment samples from the continental slope off Brazil, Uruguay, and Argentina between 20 and 48°S [*Chiessi et al.*, 2007]. By using the modern $\delta^{18}O$ gradient across the Brazil-Malvinas Confluence (BMC) and the ice volume corrected (ivc) downcore $\delta^{18}O$ record of GeoB13862-1, we estimated the latitudinal movements of the BMC (i.e., the deviation of the BMC from its present-day position in degrees of latitude). The red (blue) background indicates the modern $\delta^{18}O$ signature of the Brazil Current (Malvinas Current). We estimate the BMC latitudinal gradient to be 1.77‰/2.15° by using the difference of the latitudinal averaged $\delta^{18}O$ values of Brazil Current ($\delta^{18}O_{BC}$ = 0.99‰ between 20.61° and 35.05°S latitude) and Malvinas Current ($\delta^{18}O_{MC}$ = 2.76‰ between 37.20° and 48.91°S latitude) (red and blue lines, respectively). For error estimation, we used the minimum-maximum $\delta^{18}O$ values of Brazil Current and Malvinas Current near the transition zone (i.e., BMC) (gray edged points).

the NBS 18, 19, and 20 standards. Consequently, all $\delta^{18}O$ data given here are relative to the VPDB standard. The long-term analytical standard deviation is better than 0.07‰.

We express our $\delta^{18}O$ values as continental ice volume corrected (ivc) in order to compare our downcore $\delta^{18}O$ values to modern $\delta^{18}O$ signatures of the BC and the MC. We calculated $\delta^{18}O_{ivc}$ by using an updated version of the sea level curve of *Lambeck and Chappell* [2001] multiplied by a constant coefficient of 1.0‰/130 m [*Schrag et al.*, 2002].

By using the modern $\delta^{18}O$ gradient across the BMC [*Chiessi et al.*, 2007] and the $\delta^{18}O_{ivc}$ of GeoB13862-1, we estimated the meridional displacements of the BMC, i.e., its deviations from the confluence's modern position in degrees of latitude. We presume the BMC latitudinal gradient to be 1.77‰/2.15° by using the difference of the latitudinal averaged $\delta^{18}O$ values of BC ($\delta^{18}O_{BC}$ = 0.99‰ between 20.61° and 35.05°S) and MC ($\delta^{18}O_{MC}$ = 2.76‰ between 37.20° and 48.91°S) (Figure 3). For error estimation, we used the minimum-maximum $\delta^{18}O$ values of BC and MC near the transition zone (i.e., BMC) (Figure 3).

3.3. Spectral Analysis

Spectral analyses in the frequency domain were performed with the software REDFIT [*Schulz and Mudelsee*, 2002]. The program works directly from unevenly spaced data, avoiding the introduction of bias during interpolation. Prior to analysis, the data were linearly detrended with the software PAST [*Hammer et al.*, 2001].

3.4. Transient Holocene Climate Simulation

To assess the skill of a state-of-the-art comprehensive coupled climate model in simulating the paleo-SWW variability and to elucidate potential forcing mechanisms, we analyzed the Holocene portion of the Transient Climate Evolution (TraCE)-21 ka nonaccelerated transient simulation using the Community Climate System Model version 3 (CCSM3) [*Liu et al.*, 2009, 2014; *He*, 2011]. The model has contributed to the fourth assessment

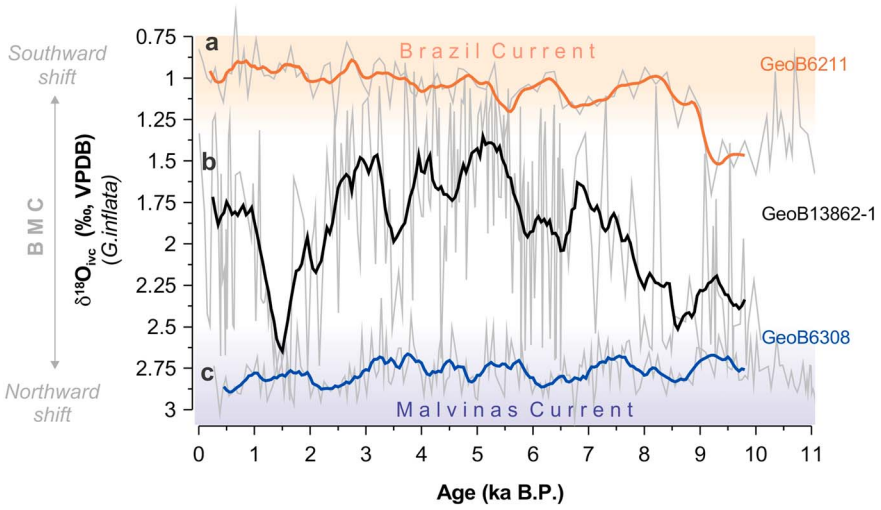

Figure 4. Ice volume corrected *Globorotalia inflata* $\delta^{18}O$ ($\delta^{18}O_{ivc}$) records along the north-south transect (thin gray lines) plotted together with a 400 year centered boxcar smoothing (bold curves). (a) $\delta^{18}O_{ivc}$ GeoB6211. Part of the record was published in *Chiessi et al.* [2013]. (b) $\delta^{18}O_{ivc}$ GeoB13862-1. (c) $\delta^{18}O_{ivc}$ GeoB6308. The red (blue) background indicates the modern $\delta^{18}O$ signature of the Brazil Current (Malvinas Current) in *G. inflata* [*Chiessi et al.*, 2007]. The low-amplitude variability of the $\delta^{18}O_{ivc}$ records of the northernmost and southernmost cores indicates that the Brazil-Malvinas Confluence never crossed ~32.5 and 39.3°S.

report of the Intergovernmental Panel on Climate Change, although the use of a lower-resolution version in the TraCE-21 ka run is owed to the length of the integration period which covers the past 21,000 years. National Center for Atmospheric Research's CCSM3 is composed of four separate components representing atmosphere, ocean, land, and sea ice [*Collins et al.*, 2006]. The resolution used in TraCE-21 ka is given by *T*31 (3.75° transform grid) in the atmosphere, with 26 layers in the vertical, while the ocean has a nominal resolution of 3° (like the sea ice component) with refined meridional resolution (0.9°) around the equator and comprises 25 levels in the vertical [*Yeager et al.*, 2006]. Starting from the Last Glacial Maximum, the model was integrated to the present subject to realistically varying forcings by orbital insolation, atmospheric greenhouse gas concentrations, continental ice sheets, and meltwater fluxes [*Liu et al.*, 2009, 2014; *He*, 2011].

4. Results

4.1. Time-Space Variability of the Brazil-Malvinas Confluence

Similar to recent observations [*Chiessi et al.*, 2007], our northernmost core shows low $\delta^{18}O_{ivc}$ values (~1.09‰) typical of the BC, whereas our southernmost core shows high $\delta^{18}O_{ivc}$ values (~2.78‰) characteristic of the MC (Figure 4). The $\delta^{18}O_{ivc}$ record of GeoB6211 (GeoB6308) thus indicates a sustained influence of the BC (MC) throughout the Holocene. Moreover, both records show only low-amplitude oscillations (≤0.5‰). In contrast, the $\delta^{18}O_{ivc}$ record of GeoB13862-1 shows high-amplitude oscillations (up to 2‰), clearly indicating alternated phases of BC and MC influence. The shifts in the $\delta^{18}O_{ivc}$ record of GeoB13862-1 can therefore be interpreted as north-south displacements of the BMC.

By using the modern $\delta^{18}O$ gradient across the BMC [*Chiessi et al.*, 2007] and the $\delta^{18}O_{ivc}$ of GeoB13862-1, we estimated the meridional displacements of the BMC, i.e., its deviations from the confluence's modern position in degrees of latitude (Figure 3). To this end, we assume that the $\delta^{18}O$ gradient across the BMC did not change significantly and that the $\delta^{18}O$ signal of the BC and the MC remained nearly constant over time. The latter assumption is validated by the GeoB6211 and GeoB6308 $\delta^{18}O$ records. However, extra caution has to be taken for the period before 9 ka B.P. because GeoB6211 indicates an elevation in $\delta^{18}O_{ivc}$ by ~0.5‰, likely implying a change in the $\delta^{18}O$ gradient across the BMC. Hence, the assumption that the end-members remain roughly constant through time seems not to be valid before 9 ka B.P., undermining the applicability of our quantitative method before 9 ka B.P. Note that, due to the "ramp-like shape" of the $\delta^{18}O$-latitude dependence (Figure 3), our quantitative approach of latitudinal shifts requires that BMC displacements are sufficiently small such that the $\delta^{18}O$ values of GeoB13862-1 remain between the GeoB6211 and GeoB6308 $\delta^{18}O$ values; i.e., GeoB13862-1 does not leave the linear $\delta^{18}O$-latitude domain of the BMC which has a width of

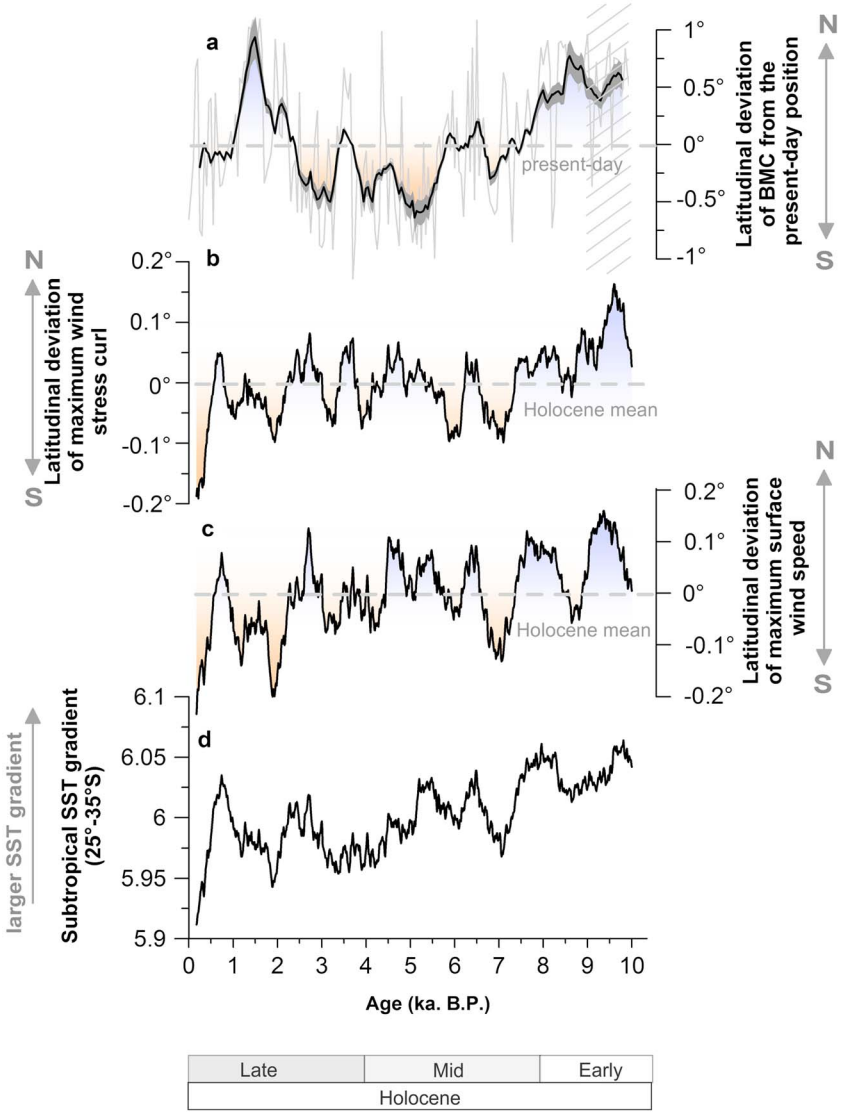

Figure 5. Comparison of proxy-based and modeled time series of meridional southern westerly winds shifts showing underestimated variability in the simulation. (a) Latitudinal deviation of the Brazil-Malvinas Confluence (BMC) (controlled by the latitude of maximum wind stress curl across the South Atlantic) from the modern position estimated from the $\delta^{18}O_{ivc}$ GeoB13862-1 record (in degrees of latitude). The gray shading represents uncertainty. The hatched area represents the interval with elevated $\delta^{18}O_{ivc}$ in core GeoB6211, likely implying a change in the $\delta^{18}O$ gradient across the BMC (see text). (b) The latitude of maximum wind stress curl zonally averaged over the South Atlantic derived from a transient CCSM3 simulation (TraCE-21 ka), expressed as the deviation from the Holocene mean. (c) The simulated latitude of maximum surface wind speed zonally averaged over the entire globe, expressed as the deviation from the Holocene mean. (d) Simulated SST difference between 25°S and 35°S (global zonal averages). All model data refer to annual means. A 400 year centered boxcar smoothing was applied to the time series.

about 2.15° (Figure 3). For millennial and longer time scales, this requirement is always fulfilled. The $\delta^{18}O_{ivc}$ record of GeoB13862-1 indicates a gradual ~1–1.5° southward shift of the BMC from the early Holocene to mid-Holocene (Figure 5a). We further observe millennial scale changes in the latitudinal position of the BMC of up to ~1° in latitude as well as substantial fluctuations at higher frequencies (Figure 5a). Spectral analysis of the time series reveals pronounced peaks at ~2500 years (i.e., 1900–3600 years) and ~250 years (Figure 6).

5. Discussion

Given the close relationship between the latitude of maximum wind stress curl across the South Atlantic and the position of the BMC, we suggest that the reconstructed north-south shifts of the BMC during the

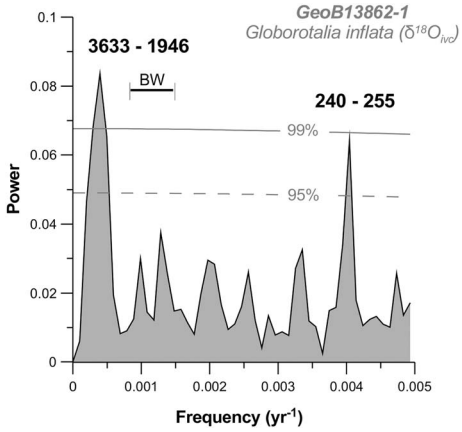

Figure 6. Spectral analysis of the ice volume corrected *Globorotalia inflata* $\delta^{18}O$ ($\delta^{18}O_{ivc}$) record of GeoB13862-1. Peaks that exceed the 95% confidence level are labeled with their periods (in years). The number of overlapping segments chosen was 3, and a rectangle-type window was used. The bandwidth (BW) indicates the frequency resolution.

Holocene were intimately linked to latitudinal shifts of the SWW and use the reconstructed BMC position as a proxy for the latitude of maximum wind stress curl [*Lumpkin and Garzoli*, 2011]. Accordingly, southward (northward) shifts of the BMC indicate decreases (increases) in the strength of the northern portion of the westerlies, consistent with southward (northward) shifts of the SWW.

However, the southward movement of the BMC from the early to mid-Holocene reconstructed here partially contradicts the results from a previous study [*Bender et al.*, 2013]. *Bender et al.* [2013] suggest the occurrence of an early Holocene northward shift of the Subtropical Shelf Front (STSF) in response to atmospheric forcing. The STSF, in turn, was claimed to be a shallow-water extension of the BMC. However, the mechanistic link between the STSF and the BMC is not well established [e.g., *Matano et al.*, 2010]. Moreover, changes in sea level play a major role on the early Holocene sedimentary dynamics in the region also affecting the position of the STSF [*Bender et al.*, 2013]. Our new data from the BMC may contribute to clarify this issue, since our records show a direct link to the position of the BMC and are not affected by changes in sea level. We therefore assume that the position of the BMC is a more conclusive proxy for the SWW, as suggested by other studies [*Peterson and Stramma*, 1991; *Matano et al.*, 1993; *Sijp and England*, 2008; *Lumpkin and Garzoli*, 2011].

Hence, considering the modern relationships between the BMC and the regional South Atlantic wind field, our data reflect a gradual ~1–1.5° southward movement of the SWW across the South Atlantic from the early to mid-Holocene. Afterward, variability in the SWW is dominated by millennial scale displacements on the order of 1° in latitude with no recognizable longer-term trend (Figure 5a).

5.1. Orbital Scale Variability of the Southern Westerly Winds Across the South Atlantic: A Proxy Model Data Approach

Orbital scale changes in insolation are the most commonly invoked driver of multimillennial scale changes in atmospheric circulation via their effect on meridional sea surface temperature (SST) gradients which might have caused long-term variations in the structure, position, and intensity of the SWW. In a multimodel study, *Varma et al.* [2012] found that long-term southward movements of the SWW are consistent with orbital forcing during the Holocene.

However, orbital scale changes of SWW during the Holocene have been discussed controversially with respect to the strength and/or position of the SWW [*Lamy et al.*, 2010; *Fletcher and Moreno*, 2012; *Kilian and Lamy*, 2012]. Validating our findings with previous reconstructions of the SWW proved to be elusive as there is a substantial incongruity between different proxy records. For the SWW core region in Patagonia (around 50°–53°S), for instance, pollen-based reconstruction of Holocene westerly-derived moisture changes suggest two opposing models of SWW changes [*Lamy et al.*, 2010; *Moreno et al.*, 2010; *Fletcher and Moreno*, 2011]. One line of evidence suggests a trend of increasing SWW strength over the Holocene [*Moreno et al.*, 2010; *Fletcher and Moreno*, 2011], while another comes to the opposite conclusion [*Lamy et al.*, 2010]. These inconsistencies may partly be related to unclear relations between precipitation and SWW strength. A local correlation map between zonal wind strength and precipitation [*Garreaud*, 2007] shows a generally weak correlation over most Southern Hemisphere landmasses for modern climate (i.e., southern Africa and southern Australia), which casts doubt on several paleo-SWW reconstructions from these regions. Hence, identifying the spatial evolution of the SWW based on a proxy record comparison alone remains difficult due to many inconsistencies or partly opposite interpretations.

In contrast to other paleo-SWW reconstruction, we focus on meridional changes of SWW characteristics (e.g., latitude of maximum SWW wind stress curl and/or SWW edges). Our approach thereby provides a method of reconstructing the integrated wind field across the entire South Atlantic (i.e., information about the

large-scale wind field), because shifts in the position of the BMC are reflected in the location of the basin-averaged wind stress curl maximum [*Lumpkin and Garzoli*, 2011], that is, a western boundary response to the latitude of maximum equatorward interior flow via sverdrup dynamics. This is an advantage over the commonly used paleohydrologic proxies, which may only provide local information about past wind field changes.

Due to the large-scale and quantitative character of our SWW reconstruction method, our data can readily be compared to climate model output. For that purpose, we calculated the latitude of maximum wind stress curl zonally averaged over the South Atlantic from the Holocene portion of the transient TraCE-21 ka simulation (Figure 5). During the early Holocene, the model simulates a gradual poleward movement of the latitude of maximum wind stress curl across the South Atlantic until ~7 ka B.P. in qualitative agreement with our proxy-inferred reconstruction of the BMC position (Figures 5a and 5b). No discernible long-term trend is simulated afterward until the onset of the industrial period when a dramatic increase in greenhouse gases causes a southward shift of the wind belt. Instead, SWW variability is dominated by millennial scale fluctuations during the middle and late (preindustrial) Holocene, again in qualitative agreement with the data. The position of the SWW core, i.e., the latitude of maximum surface wind speed, shows a similar temporal behavior as the latitude of maximum curl, indicating that changes in the latitude of maximum wind stress curl over the South Atlantic represent wholesale shifts of the SWW belt on long time scales (Figures 5b and 5c).

However, a quantitative comparison of model and proxy time series suggests that both the orbitally forced long-term early Holocene trend and the millennial scale SWW fluctuations (related to internal climate variability) are almost an order of magnitude (in terms of degrees latitude) smaller in the model than in the reconstruction. Since variations in the wind curl field across the South Atlantic are related to large-scale atmospheric dynamics, the small simulated variability cannot fully be attributed to the relatively coarse grid resolution of the global climate model. Moreover, recent model intercomparisons have shown that the magnitude of orbitally forced variations in SWW velocities in CCSM3 compares well with other global climate models [*Rojas and Moreno*, 2010; *Varma et al.*, 2012]. Our results thus suggest that state-of-the-art global climate models underestimate both orbitally forced multimillennial and internal-millennial variability of the SWW.

The latitudinal position of the SWW is influenced by SST gradients that may affect baroclinic eddy growth and momentum flux convergence through changes in tropospheric meridional temperature gradients and static stability [*Brayshaw et al.*, 2008; *Chen et al.*, 2010; *Lu et al.*, 2010; *Grise and Polvani*, 2014]. This also provides a means by which orbital forcing can drive SWW changes since varying shortwave insolation affects surface temperatures [*Varma et al.*, 2012]. *Brayshaw et al.* [2008] have shown that SST gradient anomalies close to the latitude of the subtropical jet are particularly effective at modifying midlatitude winds. An enhanced SST gradient close to the subtropical jet leads to an equatorward shift of the midlatitude eddy-driven jet and the associated surface westerlies. Figure 5d displays the temporal evolution of the meridional SST gradient around 30°S, indeed showing a high correlation with the position of the SWW. Given the importance of SST changes in driving low-frequency SWW variability, the underestimated SWW variations in the model are consistent with previous work showing that coupled atmosphere-ocean models substantially underestimate Holocene annual mean SST trends derived from alkenones [*Lohmann et al.*, 2013]. As a shift of the SWW may feedback on the SST field [*Sijp and England*, 2008], shortcomings in the simulation of surface wind variability are intimately linked to model biases in the simulation of SST variations.

5.2. Millennial Scale Variability of the Southern Westerly Winds-Northern Hemisphere Trigger and Atmospheric Teleconnection

Millennial scale variations dominate most parts of the SWW record (Figures 4 and 5a). Spectral analyses of the $\delta^{18}O_{ivc}$ record of GeoB13862-1 revealed statistically significant oscillations of ~2500 years (Figure 6). Millennial scale fluctuations at intervals of approximately 2800–2000 years are well known for the Holocene, in particular for the northern North Atlantic region [*Mayewski et al.*, 2004]. Within age-model uncertainties, the timing of millennial scale variability in the SWW seems to be synchronous with significant iceberg discharge events in the North Atlantic during the Holocene [*Bond et al.*, 2001] (Figure 7). This may indicate a pervasive link between structural changes in SWW and North Atlantic climate perturbations with southward

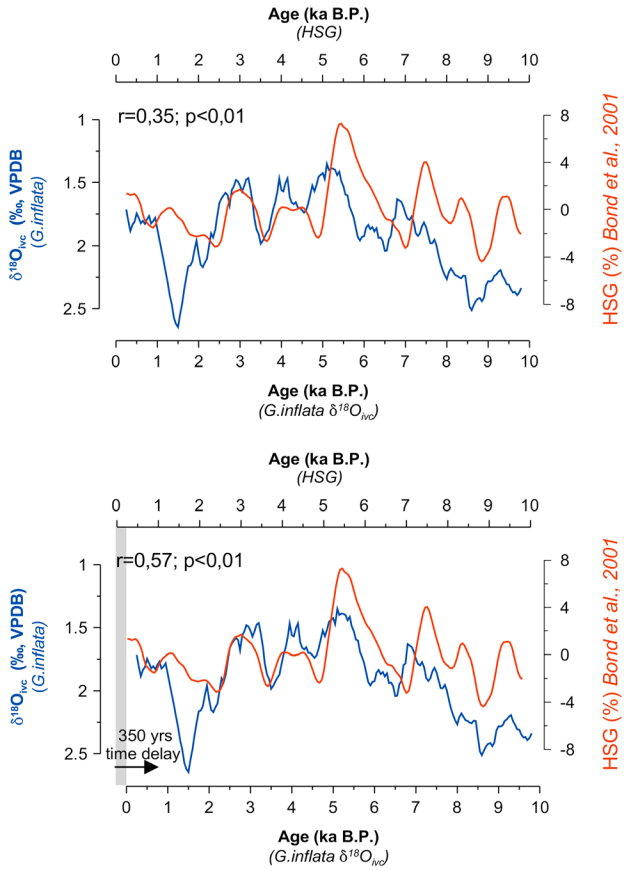

Figure 7. Comparison of the ice volume corrected $\delta^{18}O$ ($\delta^{18}O_{ivc}$) record from western South Atlantic core GeoB13862-1 with the hematite-stained grain (HSG) record from North Atlantic marine sediment cores MC52, V29191, MC21, and GGC22 [*Bond et al.*, 2001]. The blue line (red line) represents the 400 year boxcar smoothing of $\delta^{18}O_{ivc}$ GeoB13862-1 (HSG record). (a) Unchanged ($r = 0.35$, $p < 0.01$). (b) Considering a time delay of 350 years between both records ($r = 0.57$, $p < 0.01$).

shifts of the SWW corresponding to remote North Atlantic cooling. A recent model study provides a rapid mechanism by which North Atlantic cooling would be teleconnected to the SWW [*Lee et al.*, 2011]. Initial North Atlantic cooling would shift the Intertropical Convergence Zone southward along with an alteration of the Hadley circulation. A weakening of the southern branch of the Hadley circulation and subsequent weakening of the Southern Hemisphere subtropical jet would in turn modify the structure of the SWW belt and lead to a strengthening and southward shift of the SWW [*Lee and Kim*, 2003; *Lee et al.*, 2011]. A similar atmospheric teleconnection was suggested to play a key role in the atmospheric CO_2 increase during the last deglaciation [*Anderson et al.*, 2009; *Toggweiler*, 2009]. However, a possible coupling between North Atlantic climate changes and the SWW belt during the Holocene still remains speculative. Although uncertainties in age models suggest some caution on assessing lead-lag relationships during the Holocene, our $\delta^{18}O_{ivc}$ record from GeoB13862-1 shows the best correlation ($r = 0.56$, $p < 0.01$) to the North Atlantic drift-ice record [*Bond et al.*, 2001] when a time delay of 350 years is considered (Figure 7). Other mechanisms might also have produced SWW millennial scale reorganizations, in particular through oceanic pathways [*Knutti et al.*, 2004]. In order to appropriately scrutinize this issue, the development of high temporal resolution and precisely dated palaeoenvironmental records from the tropics would be of paramount importance. This will help to determine whether atmospheric processes or oceanic mechanisms acted as a pacemaker for interhemispheric abrupt Holocene climate changes.

6. Conclusion

Here we present high temporal resolution planktonic foraminifera $\delta^{18}O$ records from the western South Atlantic that reveal Holocene orbital-to-millennial scale migrations of the BMC, a highly sensitive feature for changes in the position and strength of the northern portion of the SWW. Through the tight coupling of the BMC to the regional wind field, this study allows for the first time reconstructing Holocene temporal and spatial evolution of the SWW across the South Atlantic. Our data suggest a gradual orbitally forced ~1–1.5° poleward movement of the SWW during the early to mid-Holocene. Afterward, variability in the SWW is dominated by millennial scale displacements on the order of 1° in latitude with no discernible long-term trend. The temporal and spatial evolution of the SWW during the Holocene is, given their importance for regional and global climate, a significant challenge to climate modeling attempts at predicting future climate change in the Southern Hemisphere extratropics. Climate models predict a southward movement of the SWW by about 1° of latitude in response to a doubling of atmospheric CO_2 [*Russell et al.*, 2006]. The results presented in this study suggest that natural millennial scale variability of the SWW position is of the same

order of magnitude, while climate models tend to substantially underestimate natural variability at these time scales. Modeled projections of future SWW shifts are therefore highly uncertain given the potential interference of anthropogenic changes in the zonal winds with internal low-frequency variability barely captured by general circulation models.

Acknowledgments

We thank M. Segl for the help with the isotope analyses. We also thank A.R. Piola for the discussion and two anonymous reviewers for their constructive comments. This study was funded through the DFG-Research Center/Cluster of Excellence "The Ocean in the Earth System" and was supported by GLOMAR–Bremen International Graduate School for Marine Sciences. C.M.C. acknowledges the support from FAPESP (2010/09983-9 and 2012/17517-3). We thank F. He, Z. Liu, and B. Otto-Bliesner for making available the TraCE-21 ka model output via the Earth System Grid (National Center for Atmospheric Research). The data of this study are available in the PANGAEA database (http://doi.pangaea.de/10.1594/PANGAEA.841893).

References

Anderson, R., S. Ali, and L. Bradtmiller (2009), Wind-driven upwelling in the Southern Ocean and the deglacial rise in atmospheric CO_2, *Science*, *323*(5920), 1443–1448.

Bender, V. B., T. J. J. Hanebuth, and C. M. Chiessi (2013), Holocene shifts of the Subtropical Shelf Front off southeastern South America controlled by high and low latitude atmospheric forcings, *Paleoceanography*, *28*, 481–490, doi:10.1002/palo.20044.

Bleil, U., et al. (2001), Report and preliminary results of Meteor Cruise M46/3, Montevideo-Mar del Plata, January 4–February 7, 2000, *Berichte Fachbereich Geowissenschaften*, 172, 161 pp.

Bond, G., B. Kromer, J. Beer, R. Muscheler, M. N. Evans, W. Showers, S. Hoffmann, R. Lotti-Bond, I. Hajdas, and G. Bonani (2001), Persistent solar influence on North Atlantic climate during the Holocene, *Science*, *294*(5549), 2130–2136, doi:10.1126/science.1065680.

Brayshaw, D. J., B. Hoskins, and M. Blackburn (2008), The storm-track response to idealized SST perturbations in an aquaplanet GCM, *J. Atmos. Sci.*, *65*(9), 2842–2860, doi:10.1175/2008JAS2657.1.

Chen, G., R. A. Plumb, and J. Lu (2010), Sensitivities of zonal mean atmospheric circulation to SST warming in an aquaplanet model, *Geophys. Res. Lett.*, *37*, L12701, doi:10.1029/2010GL043473.

Chiessi, C. M., S. Ulrich, S. Mulitza, J. Pätzold, and G. Wefer (2007), Signature of the Brazil-Malvinas Confluence (Argentine Basin) in the isotopic composition of planktonic foraminifera from surface sediments, *Mar. Micropaleontol.*, *64*(1–2), 52–66, doi:10.1016/j.marmicro.2007.02.002.

Chiessi, C. M., S. Mulitza, A. Paul, J. Pätzold, J. Groeneveld, and G. Wefer (2008), South Atlantic interocean exchange as the trigger for the Bølling warm event, *Geology*, *36*(12), 919, doi:10.1130/G24979A.1.

Chiessi, C. M., S. Mulitza, J. Groeneveld, J. B. Silva, M. C. Campos, and M. H. C. Gurgel (2013), Variability of the Brazil Current during the late Holocene, *Palaeogeogr. Palaeoclimatol. Palaeoecol.*, *415*, 28–36, doi:10.1016/j.palaeo.2013.12.005.

Collins, W. D., et al. (2006), The Community Climate System Model version 3 (CCSM3), *J. Clim.*, *19*, 2122–2143.

Fletcher, M.-S., and P. I. Moreno (2011), Zonally symmetric changes in the strength and position of the southern westerlies drove atmospheric CO_2 variations over the past 14 kyr, *Geology*, *39*(5), 419–422, doi:10.1130/G31807.1.

Fletcher, M.-S., and P. I. Moreno (2012), Have the southern westerlies changed in a zonally symmetric manner over the last 14,000 years? A hemisphere-wide take on a controversial problem, *Quat. Int.*, *253*, 32–46, doi:10.1016/j.quaint.2011.04.042.

Franke, J., A. Paul, and M. Schulz (2008), Modeling variations of marine reservoir ages during the last 45,000 years, *Clim. Past*, *4*, 125–136.

Garreaud, R. (2007), Precipitation and circulation covariability in the extratropics, *J. Clim.*, *20*(18), 4789–4797, doi:10.1175/JCLI4257.1.

Garzoli, S., and C. Giulivi (1994), What forces the variability of the southwestern Atlantic boundary currents?, *Deep Sea Res.*, *41*(10), 1527–1550.

Garzoli, S. L., and A. Bianchi (1987), Time-space variability of the local dynamics of the Malvinas-Brazil Confluence as revealed by inverted echo sounders, *J. Geophys. Res.*, *92*(C2), 1914–1922, doi:10.1029/JC092iC02p01914.

Garzoli, S. L., and Z. Garraffo (1989), Transports, frontal motions, and eddies at the Brazil-Malvinas currents confluence, *Deep Sea Res.*, *36*(5), 681–703, doi:10.1016/0198-0149(89)90145-3.

Goni, G. J., and I. Wainer (2001), Investigation of the Brazil Current front variability from altimeter data, *J. Geophys. Res.*, *106*(C12), 31,117–31,128, doi:10.1029/2000JC000396.

Gordon, A. (1981), South Atlantic thermocline ventilation, *Deep Sea Res.*, *28*(11), 1239–1264.

Grise, K. M., and L. M. Polvani (2014), The response of midlatitude jets to increased CO_2: Distinguishing the roles of sea surface temperature and direct radiative forcing, *Geophys. Res. Lett.*, *41*, 6863–6871, doi:10.1002/2014GL061638.

Groeneveld, J., and C. M. Chiessi (2011), Mg/Ca of *Globorotalia inflata* as a recorder of permanent thermocline temperatures in the South Atlantic, *Paleoceanography*, *26*, PA2203, doi:10.1029/2010PA001940.

Hammer, Ø., D. A. T. Harper, and P. D. Ryan (2001), PAST: Paleontological statistics software package for education and data analysis, *Palaeontol. Electron.*, *4*, 9.

He, F. (2011), Simulating transient climate evolution of the last deglaciation with CCSM3, PhD thesis, Univ. of Wisconsin-Madison, Madison.

Jenny, B., D. Wilhelm, and B. Valero-Garcés (2003), The southern westerlies in central Chile: Holocene precipitation estimates based on a water balance model for Laguna Aculeo (33°50'S), *Clim. Dyn.*, *20*, 269–280, doi:10.1007/s00382-002-0267-3.

Kalnay, E., et al. (1996), The NCEP/NCAR 40 year reanalysis project, *Bull. Am. Meteorol. Soc.*, *77*, 437–471.

Kilian, R., and F. Lamy (2012), A review of glacial and Holocene paleoclimate records from southernmost Patagonia (49–55°S), *Quat. Sci. Rev.*, *53*, 1–23, doi:10.1016/j.quascirev.2012.07.017.

Knutti, R., J. Flückiger, T. F. Stocker, and A. Timmermann (2004), Strong hemispheric coupling of glacial climate through freshwater discharge and ocean circulation, *Nature*, *430*(7002), 851–856, doi:10.1038/nature02786.

Kohfeld, K. E., R. M. Graham, A. M. de Boer, L. C. Sime, E. W. Wolff, C. Le Quéré, and L. Bopp (2013), Southern Hemisphere westerly wind changes during the Last Glacial Maximum: Paleodata synthesis, *Quat. Sci. Rev.*, *68*, 76–95, doi:10.1016/j.quascirev.2013.01.017.

Krastel, S., and G. Wefer (2012), Report and preliminary results of RV Meteor Cruise M78/3. Sediment transport off Uruguay and Argentina: From the shelf to the deep sea; 19 05 2009–06 07 2009, Montevideo, *Berichte Fachbereich Geowissenschaften*, 285, 79 pp.

Lambeck, K., and J. Chappell (2001), Sea level change through the last glacial cycle, *Science*, *292*(5517), 679–686, doi:10.1126/science.1059549.

Lamy, F., R. Kilian, H. W. Arz, J.-P. Francois, J. Kaiser, M. Prange, and T. Steinke (2010), Holocene changes in the position and intensity of the southern westerly wind belt, *Nat. Geosci.*, *3*(10), 695–699, doi:10.1038/ngeo959.

Lantzsch, H., T. J. J. Hanebuth, C. M. Chiessi, T. Schwenk, and R. A. Violante (2014), The high-supply, current-dominated continental margin of southeastern South America during the late Quaternary, *Quat. Res.*, *81*(2), 339–354, doi:10.1016/j.yqres.2014.01.003.

Lee, S., and H. Kim (2003), The dynamical relationship between subtropical and eddy-driven jets, *J. Atmos. Sci.*, *60*, 1490–1503.

Lee, S.-Y., J. C. H. Chiang, K. Matsumoto, and K. S. Tokos (2011), Southern Ocean wind response to North Atlantic cooling and the rise in atmospheric CO_2: Modeling perspective and paleoceanographic implications, *Paleoceanography*, *26*, PA1214, doi:10.1029/2010PA002004.

Liu, Z., et al. (2009), Transient simulation of last deglaciation with a new mechanism for Bølling-Allerød warming, *Science*, *325*(5938), 310–314, doi:10.1126/science.1171041.

Liu, Z., J. Zhu, Y. Rosenthal, X. Zhang, B. L. Otto-Bliesner, A. Timmermann, R. S. Smith, G. Lohmann, W. Zheng, and O. Elison Timm (2014), The Holocene temperature conundrum, *Proc. Natl. Acad. Sci.*, *111*(34), E3501–E3505, doi:10.1073/pnas.1407229111.

Lohmann, G., M. Pfeiffer, T. Laepple, G. Leduc, and J.-H. Kim (2013), A model-data comparison of the Holocene global sea surface temperature evolution, *Clim. Past*, *9*(4), 1807–1839, doi:10.5194/cp-9-1807-2013.
Lončarić, N., F. J. C. Peeters, D. Kroon, and G.-J. A. Brummer (2006), Oxygen isotope ecology of recent planktic foraminifera at the central Walvis Ridge (SE Atlantic), *Paleoceanography*, *21*, PA3009, doi:10.1029/2005PA001207.
Lu, J., G. Chen, and D. M. W. Frierson (2010), The position of the midlatitude storm track and eddy-driven westerlies in aquaplanet AGCMs, *J. Atmos. Sci.*, *67*(12), 3984–4000, doi:10.1175/2010JAS3477.1.
Lumpkin, R., and S. Garzoli (2011), Interannual to decadal changes in the western South Atlantic's surface circulation, *J. Geophys. Res.*, *116*, C01014, doi:10.1029/2010JC006285.
Matano, R. P., E. D. Palma, and A. R. Piola (2010), The influence of the Brazil and Malvinas Currents on the southwestern Atlantic Shelf circulation, *Ocean Sci.*, *6*(4), 983–995, doi:10.5194/os-6-983-2010.
Matano, R., M. Schlax, and D. Chelton (1993), Seasonal variability in the southwestern Atlantic, *J. Geophys. Res.*, *98*(C10), 18,027–18,035, doi:10.1029/93JC01602.
Mayewski, P. A., et al. (2004), Holocene climate variability, *Quat. Res.*, *62*(3), 243–255, doi:10.1016/j.yqres.2004.07.001.
Moreno, P. I. (2004), Millennial scale climate variability in northwest Patagonia over the last 15,000 years, *J. Quaternary Sci.*, *19*(1), 35–47, doi:10.1002/jqs.813.
Moreno, P. I., J. P. Francois, C. M. Moy, and R. Villa-Martinez (2010), Covariability of the southern westerlies and atmospheric CO_2 during the Holocene, *Geology*, *38*(8), 727–730, doi:10.1130/G30962.1.
Moros, M., P. De Deckker, E. Jansen, K. Perner, and R. J. Telford (2009), Holocene climate variability in the Southern Ocean recorded in a deep-sea sediment core off South Australia, *Quat. Sci. Rev.*, *28*(19–20), 1932–1940, doi:10.1016/j.quascirev.2009.04.007.
Nicholson, S., and H. Flohn (1980), African environmental and climatic changes and the general atmospheric circulation in late Pleistocene and Holocene, *Clim. Change*, *2*, 313–348.
Oke, P., and M. England (2004), Oceanic response to changes in the latitude of the Southern Hemisphere subpolar westerly winds, *J. Clim.*, *17*, 1040–1054.
Olson, D., G. Podestá, R. Evans, and O. Brown (1988), Temporal variations in the separation of Brazil and Malvinas Currents, *Deep Sea Res.*, *35*(12), 1971–1990.
Peterson, R., and L. Stramma (1991), Upper level circulation in the South Atlantic Ocean, *Prog. Oceanogr.*, *26*, 1–73.
Razik, S., C. M. Chiessi, O. E. Romero, and T. von Dobeneck (2013), Interaction of the South American monsoon system and the southern westerly wind belt during the last 14 kyr, *Palaeogeogr. Palaeoclimatol. Palaeoecol.*, *374*, 28–40, doi:10.1016/j.palaeo.2012.12.022.
Reimer, P., M. Baillie, and E. Bard (2009), IntCal09 and Marine09 radiocarbon age calibration curves, 0–50,000 cal years B.P, *Radiocarbon*, *51*, 1111–1150.
Rojas, M., and P. I. Moreno (2010), Atmospheric circulation changes and neoglacial conditions in the Southern Hemisphere midlatitudes: Insights from PMIP2 simulations at 6 kyr, *Clim. Dyn.*, *37*(1–2), 357–375, doi:10.1007/s00382-010-0866-3.
Russell, J. L., K. W. Dixon, A. Gnanadesikan, R. J. Stouffer, and J. R. Toggweiler (2006), The Southern Hemisphere westerlies in a warming world: Propping open the door to the deep ocean, *J. Clim.*, *19*, 6382–6390.
Saraceno, M., C. Provost, A. R. Piola, J. Bava, and A. Gagliardini (2004), Brazil Malvinas frontal system as seen from 9 years of advanced very high resolution radiometer data, *J. Geophys. Res.*, *109*, C05027, doi:10.1029/2003JC002127.
Schrag, D. P., J. F. Adkins, K. McIntyre, J. L. Alexander, D. A. Hodell, C. D. Charles, and J. F. McManus (2002), The oxygen isotopic composition of seawater during the Last Glacial Maximum, *Quat. Sci. Rev.*, *21*(1–3), 331–342, doi:10.1016/S0277-3791(01)00110-X.
Schulz, K., et al. (2001), Report and preliminary results of Meteor Cruise M46/2, Recife (Brazil)–Montevideo (Uruguay), December 2–December 29, 1999, *Berichte Fachbereich Geowissenschaften*, 174, 107 pp.
Schulz, M., and M. Mudelsee (2002), REDFIT: Estimating red-noise spectra directly from unevenly spaced paleoclimatic time series, *Comput. Geosci.*, *28*(3), 421–426, doi:10.1016/S0098-3004(01)00044-9.
Shulmeister, J. (1999), Australasian evidence for mid-Holocene climate change implies precessional control of Walker circulation in the Pacific, *Quat. Int.*, *58*, 81–91.
Shulmeister, J., et al. (2004), The Southern Hemisphere westerlies in the Australasian sector over the last glacial cycle: A synthesis, *Quat. Int.*, *118–119*, 23–53, doi:10.1016/S1040-6182(03)00129-0.
Sijp, W. P., and M. H. England (2008), The effect of a northward shift in the Southern Hemisphere westerlies on the global ocean, *Prog. Oceanogr.*, *79*(1), 1–19, doi:10.1016/j.pocean.2008.07.002.
Sime, L. C., K. E. Kohfeld, C. Le Quéré, E. W. Wolff, A. M. de Boer, R. M. Graham, and L. Bopp (2013), Southern Hemisphere westerly wind changes during the Last Glacial Maximum: Model-data comparison, *Quat. Sci. Rev.*, *64*, 104–120, doi:10.1016/j.quascirev.2012.12.008.
Thompson, D. W. J., and S. Solomon (2002), Interpretation of recent Southern Hemisphere climate change, *Science*, *296*(5569), 895–899, doi:10.1126/science.1069270.
Toggweiler, J. (2009), Shifting westerlies, *Science*, *323*(5920), 1434–1435.
Toggweiler, J., and B. Samuels (1995), Effect of Drake Passage on the global thermohaline circulation, *Deep Sea Res.*, *42*(4), 477–500.
Varma, V., M. Prange, U. Merkel, T. Kleinen, G. Lohmann, M. Pfeiffer, H. Renssen, A. Wagner, S. Wagner, and M. Schulz (2012), Holocene evolution of the Southern Hemisphere westerly winds in transient simulations with global climate models, *Clim. Past*, *8*(2), 391–402, doi:10.5194/cp-8-391-2012.
Voigt, I., R. Henrich, B. Preu, A. Piola, T. J. J. Hanebuth, S. Tillmann, and C. M. Chiessi (2013), A submarine canyon as a climate archive interaction of the Antarctic Intermediate Water with the Mar del Plata Canyon (Southwest Atlantic), *Mar. Geol.*, *341*, 46–57, doi:10.1016/j.margeo.2013.05.002.
Yeager, S. G., C. A. Shields, W. G. Large, and J. J. Hack (2006), The low-resolution CCSM3, *J. Clim.*, *19*(2004), 2545–2566.